

Prototype Lead Tungstate Calorimeter Test for TPEX

I. Frišćić,^{1,*} E. Cline,² J.C. Bernauer,^{2,3} D.K. Hasell,¹ R. Johnston,¹

I. Lavrukhin,⁴ S. Lee,¹ P. Moran,¹ and U. Schneekloth⁵

¹*Laboratory for Nuclear Science, Massachusetts Institute of Technology, Cambridge, MA, 02139, USA*

²*Center for Frontiers in Nuclear Science, Department of Physics and Astronomy,
Stony Brook University, Stony Brook, NY, 11794, USA*

³*RIKEN BNL Research Center, Brookhaven National Laboratory, Upton, NY, 11973, USA*

⁴*Randall Laboratory of Physics, University of Michigan, Ann Arbor, MI 48109, USA*

⁵*Deutsches Elektronen-Synchrotron DESY, Germany*

Tests of a prototype lead tungstate calorimeter were made over two weeks at the end of September, 2019, at the DESY II Test Beam Facility in Hamburg, Germany. The purpose of these tests was to gain experience with the construction, operation, and performance of a simple lead tungstate calorimeter, and also to compare a traditional triggered readout scheme with a streaming readout approach. These tests are important for the proposed Two-Photon Exchange experiment at the DESY test beam facility and for work towards a future electromagnetic calorimeter that could be used in an Electron-Ion Collider detector. Details on all aspects of the test, the subsequent analysis, and the results are presented.

CONTENTS

I. Introduction	1
II. Exp-Setup	2
III. Analysis Methodology	2
A. Deposited energy and linearity	2
IV. Streaming and triggered readout	4
V. Simulation of Test Beam	6
VI. Conclusions	7
VII. Acknowledgements	7
References	8

I. INTRODUCTION

A prototype lead tungstate calorimeter was assembled at MIT and shipped to the DESY laboratory in Hamburg, Germany where numerous tests were performed at the DESY II Test Beam Facility [1]. These tests were part of an R&D program to study lead tungstate calorimeters in preparation for the Two-Photon Exchange eXperiment (TPEX) proposed for the DESY II Test Beam Facility and for a future electromagnetic calorimeter under consideration as part of an Electron-Ion Collider (EIC) detector [2].

The aim of the TPEX measurements is to determine the contribution of “hard” two-photon exchange in lepton-proton elastic scattering. Two-photon exchange

is the leading explanation for the observed discrepancy between proton form factor ratio, $\mu_p G_E^p / G_M^p$, measurements using Rosenbluth separation and polarization transfer techniques. An in-depth review can be found in [3]. Previous measurements [4, 5] observed a small ($\sim 1\%$) “hard” two-photon exchange contribution but were limited to relatively low Q^2 (< 2.1 (GeV/c)²) where the proton form factor discrepancy is not clear. TPEX would make measurements at Q^2 up to 4.6 (GeV/c)² where the discrepancy is more obvious. Measurements at higher momentum transfers would also be possible with some detector improvements. Lead tungstate calorimeters have excellent energy resolution which would help identify elastic lepton scattering from the background of recoil protons, pion production, and other processes.

The excellent energy resolution is also the reason behind its selection as part of the back angle electromagnetic calorimeter (EMCal) for an EIC detector [2]. Nearly all EIC physics processes require detecting the scattered electron. Measuring the energy of back-angle scattered electrons is crucial for determining the kinematics of inclusive and semi-inclusive deep inelastic scattering. It is likely that lead tungstate crystals will be used in the small angle region of the EMCal where the electron energies are small but the rates are high.

In addition to studying the performance of the lead tungstate calorimeter two parallel readout schemes were used for data acquisition. These were: a traditional triggered readout scheme and a streaming readout scheme. The aim for this was to directly compare the results from the two schemes to identify any issues that may need to be addressed in the future. Streaming readout is not required for the TPEX measurements as the time between bunches will be large (~ 80 ms) leaving sufficient time to readout the detectors using a simple trigger based on the beam bunch clock. However, at the EIC streaming readout is widely accepted as the preferred and necessary approach to readout the large number channels from various detectors and present the data in a coordinated

* friscic@mit.edu; ifrisic@phy.hr; Present address: Department of Physics, PMF, University of Zagreb, Croatia.

fashion to the clusters of computers that will select valid events and perform event reconstruction.

The experimental setup and test procedures are briefly described below. This is followed by a description of the analysis including a comparison of the results from the two readout schemes. The calorimeter performance is also compared to Monte Carlo Geant4 [6, 7] simulations to verify our understanding of the lead tungstate calorimeters. Finally some conclusions are drawn and plans for future tests are presented.

II. EXP-SETUP

The calorimeter used in the initial test run consisted of nine $2 \times 2 \times 20$ cm lead tungsten crystals from a set of 27 lead tungstate crystals [8, 9] generously loaned to us by Tanja Horn from the Catholic University of America. The light produced in each crystal was detected using Hamamatsu R1166 PMTs attached to one end of the crystal. The rest of the crystal surface was wrapped with one layer of white Tyvek (0.4 mm thick) to aid internal reflection and then wrapped with one layer of opaque aluminum foil (0.09 mm thick) to prevent light leakage and cross-talk. The crystal-PMT assembly was placed inside an anodized aluminum housing in 3×3 configuration. SHV and BNC feedthrough connectors for high voltage and signal were mounted on opposing sides of the box. Two $1/4$ " flexible copper tubes were pressed into machined tracks around the central part of the box. The copper pipes were connected to a cooling water loop.

The calorimeter assembly was mounted on a 2D-moving table in front of the trigger detector set-up and the opening for the electron beam, see Fig. 1. A laser cross indicating the electron beam position was used to determine coordinates for the center of each crystal. When looking downstream into the front face of the calorimeter the crystals are numbered from 0 to 8 starting from the top left.

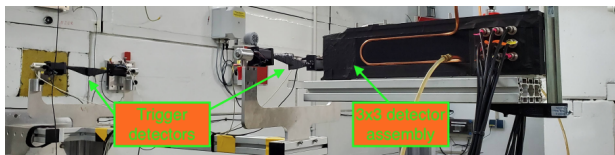


Figure 1. Photo of 3x3 lead tungstate calorimeter prototype and trigger detectors used in initial test run at DESY.

Power to the PMTs was provided by LeCroy 1461N modules housed in a LeCroy 1458 HV mainframe. Each LeCroy 1461N module has 12 independent SHV outputs providing up to -3 kV and 2.5 mA.

A block diagram of the readout setup for a single calorimeter crystal is shown in Fig. 2. Signals from the PMTs were connected to a signal splitter. One output was read out in streaming mode by a CAEN V1725 wave-

form digitizer, having 14-bit resolution and 250 MS/s sampling rate. Since this model of the digitizer has 8 channels, a decision was made to read out crystals 1 to 7, and use channel 0 for the trigger signal. For each detected signal, the following information was saved to disk: the waveform, the channel number, online extracted energy from the full acquisition window width, online extracted energy from the shorter acquisition window width, time stamp (4 ns resolution), and PC time in seconds and in nanoseconds when the data stream from the digitizer arrived to be saved to PC.

The other output of the signal splitter was read out by a classical triggered readout system. Therefore, the signal was first delayed by 100 ns to fit into the window defined by the trigger signal and then read out using the CAEN V792 32 channel 12-bit QDC. For each trigger signal all channels were read out and the following information were saved to the PC: the channel number and the corresponding energy, and PC time in seconds and in nanoseconds when the data for a particular trigger signal have been recorded to PC.

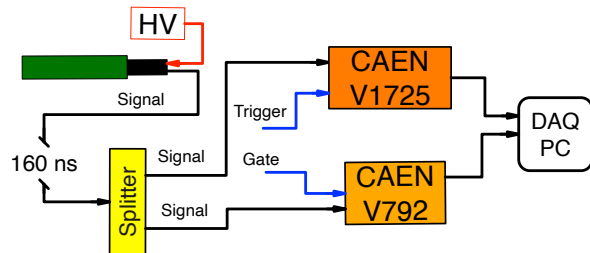


Figure 2. The block diagram of the readout setup for a single calorimeter crystal.

III. ANALYSIS METHODOLOGY

A. Deposited energy and linearity

Before taking the test data each PMT's HV was adjusted to produce approximately the same amplitude of signal (gain matched). For this, the translation table was adjusted to center the electron beam on the center of each crystal and data was collected with a 5.2 GeV electron beam. The high voltage for the selected crystal was adjusted to yield a peak in the QDC energy spectrum close to end of the QDC energy range with as little overflow as possible.

Data was collected at four different beam energies: 2, 3, 4, and 5 GeV and with the translation table adjusted to center the beam on each crystal. This data was subsequently used to determine a more precise normalisation for the gain of each crystal. It also provided a measure of the linearity of the response versus energy.

Lateral and vertical scans (± 2 cm) were then made at the same four beam energies over the center crystal to study the response versus beam position. Two different collimator size (2×2 mm and 8×8 mm) were used as well as with and without 1 cm and 2 cm thick lead absorbers in front of the calorimeter.

A plot of typical energy spectra for all four beam energies can be seen in Fig. 3. The top panel shows the QDC spectra (with pedestal subtraction) and the bottom panel shows digitizer spectra for events which are in coincidence with the trigger signal.

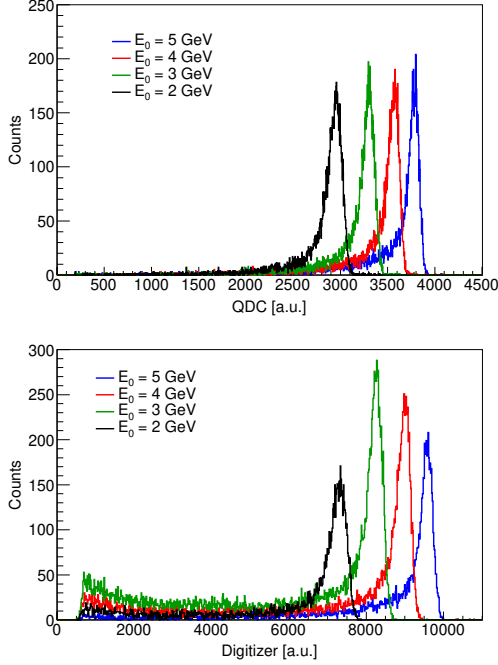


Figure 3. Deposited energy in central crystal recorded by the QDC (top) and the digitizer (bottom) in central crystal. The events shown in the digitizer spectra also required a coincidence with a trigger signal in channel 0 of the digitizer.

When a high energy electron from the beam hits the crystal it will produce a particle shower which is not necessarily contained in a single crystal. In order to reconstruct the full energy of the particle one needs to sum deposited energy in all crystals for this particular event. Figure 4 shows an example of this sum when the 5 GeV beam was directed at the central crystal. ROOT functions "gaus" and "crystalball" were used to extract the position of the peak. As can be seen, the "crystalball" function better fits the shape of the histogram than the "gaus" function.

Positions of the sum peaks for all four energies were plotted against beam energies in Fig. 5. We can see that the data is not perfectly linear and with increasing beam energy more of the particle shower energy is lost between the crystals.

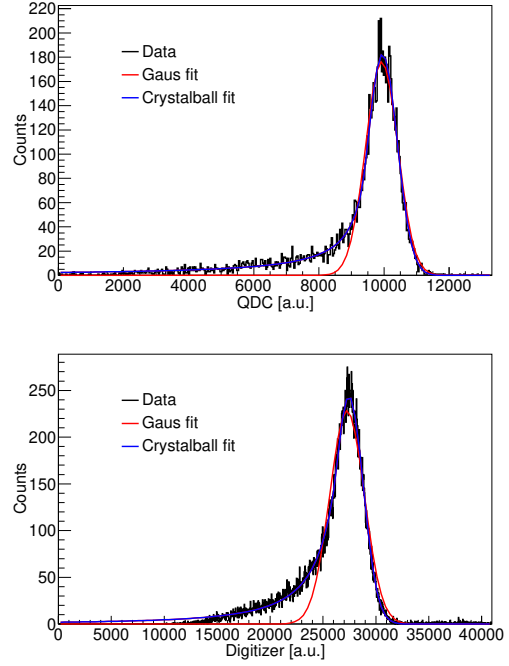


Figure 4. Sum of energies deposited in all crystals recorded by the QDC and the digitizer when 5 GeV electron beam was centered at crystal 4. The events shown in digitizer spectra also required a coincidence with a trigger signal in channel 0 of the digitizer.

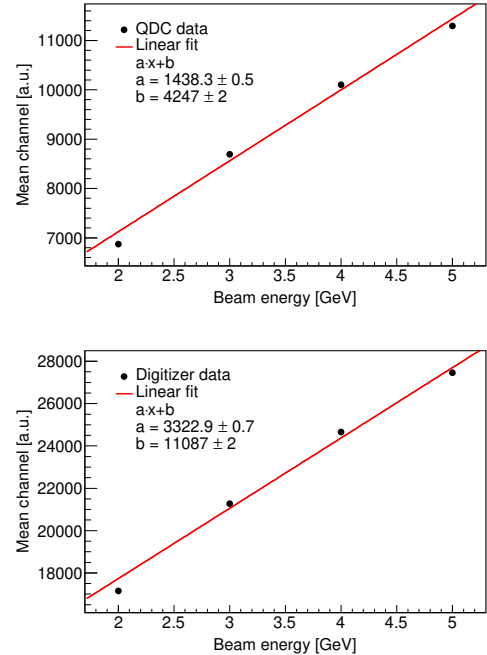


Figure 5. Energy dependence of the peak position of the energy spectra sum in the QDC and the digitizer. The peak position is defined as the mean value extracted from the crystal ball fit.

IV. STREAMING AND TRIGGERED READOUT

Due to QDC limitations, like dead time, requiring the trigger signal, etc., the QDC accepts a lower event rate than the digitizer. To account for this difference in recorded events, the data recorded by the digitizer without trigger signal was removed from the analysis. Below we show our technique for removing these events for a 2 GeV electron beam run with the beam centered on the central crystal.

The digitizer accepts all events above a threshold. These events must be correlated with the trigger signal. This was done by determining two time differences: for all events in a selected crystal between two subsequent events in channel 0 (trigger signal) one time difference was formed with first channel 0 event and the other with the second channel 0 event. In other words, time difference of events before event in channel 0 and the time difference of events after channel 0, as can be seen in Fig. 6 for central crystal (channel 4). The similar timing offset was also found for other channels.

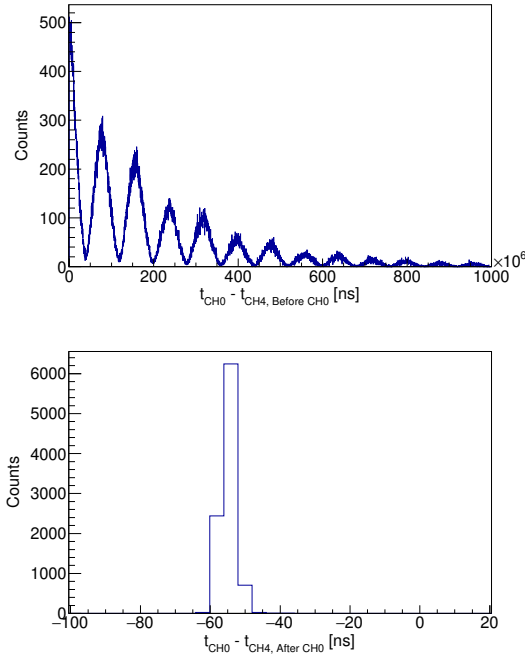


Figure 6. Time difference between the channel 4 and trigger signal in channel 0. The upper panel shows the time difference for events in channel 4 that occurred before the trigger, and the bottom panel shows events that occurred after the trigger signal. The regular structure that occurs in the top panel corresponds to the 12.5 Hz frequency when the beam enters the experimental hall.

The events forming a coincidence with channel 0 were identified. The same procedure, as explained above, was used to determine the coincidence between events from

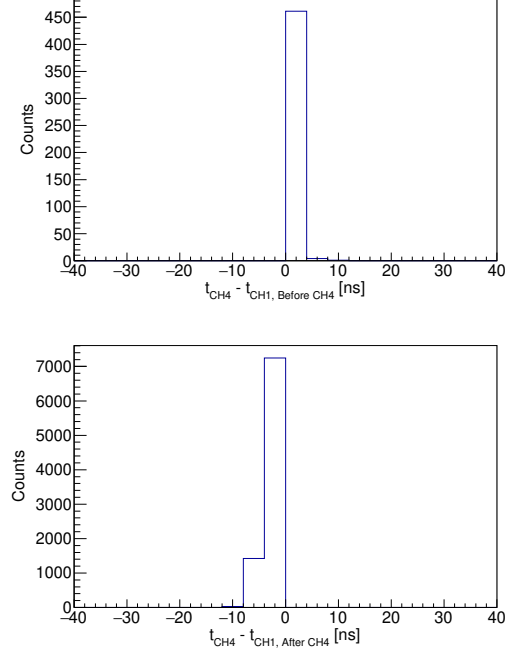


Figure 7. Time difference between the channel 4 and channel 1 if the signal in channel 1 is recorded before (top) or after (bottom) the signal in channel 4.

different crystals. Figure 7 clearly shows that these coincidences exist and the time offset between events in channel 4 and channel 1. Other channels had similar offset with channel 4.

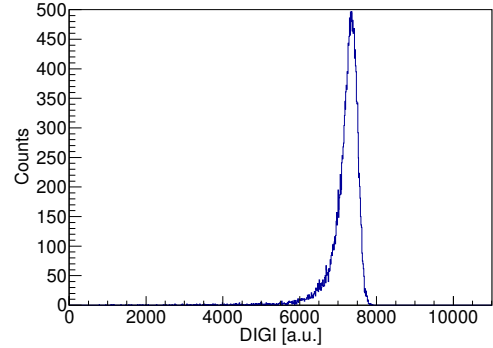


Figure 8. Deposited energy in central detector (channel 4) for events which are in coincidence with at least 6 other events either in the digitizer channels or the trigger signal.

Using the determined time offsets for channel 4, the original data sample was searched for all events which are in agreement with these offsets. Figure 8 shows all the selected events in the central crystal which are in coincidence with at least 6 other events either in digitizer channels or the trigger signal. The number of such events

(21452 events) is more than two times larger than the total number of trigger events recorded by the QDC (9971 events) for this particular run. Showing a clear advantage of streaming readout compared to "classical" triggered readout.

In approximately 4 % of the events recorded by the digitizer, there was an error in the readout indicating that the digitizer conversion was not finished. This was a random occurrence during a run, so when selecting events in the digitizer that also had a trigger, we saw 4 % fewer events than in the QDC.

Considering that the same data was measured with two different data acquisition schemes, the question arose if we can clearly identify events recorded in QDC in the huge amount of data recorded by the digitizer (approx. 190000 in the same crystal).

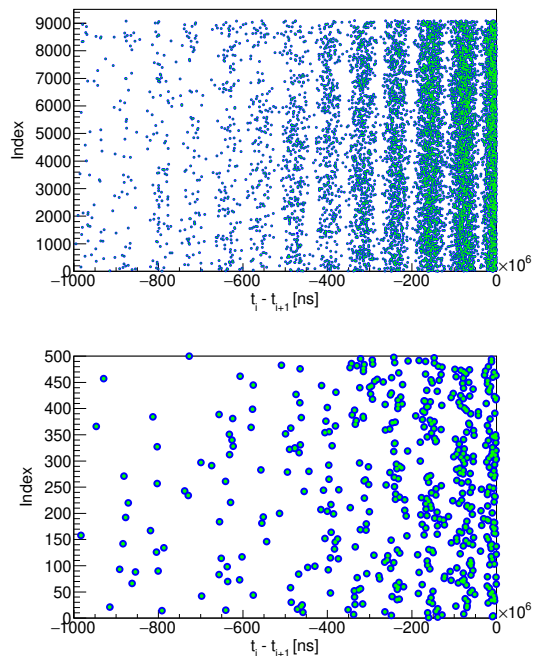


Figure 9. Time interval between subsequent events in QDC (green points) and in digitizer (blue points). The upper panel shows the full range in number of time intervals. In order to show the good agreement between the QDC and the digitizer data, the size of the blue points was exaggerated and the bottom panel shows only the first 500 time intervals.

Both the QDC and the digitizer are read out by their own software which can be started independently from each other. The clock which defines the timing for the QDC data recording is totally asynchronous from the clock defining the timing for the digitizer data recording which is also asynchronous with the digitizer's own time stamps. This means that for each new run one would need to determine a new time offset between the clocks. In order to avoid this complication, the solution is to calculate the time difference between the subsequent events

in QDC and digitizer data. The next step is to correct the 4 % smaller number of digitizer coincidence events compared to QDC and one obtains data with excellent time alignment in both readout schemes shown in Fig. 9.

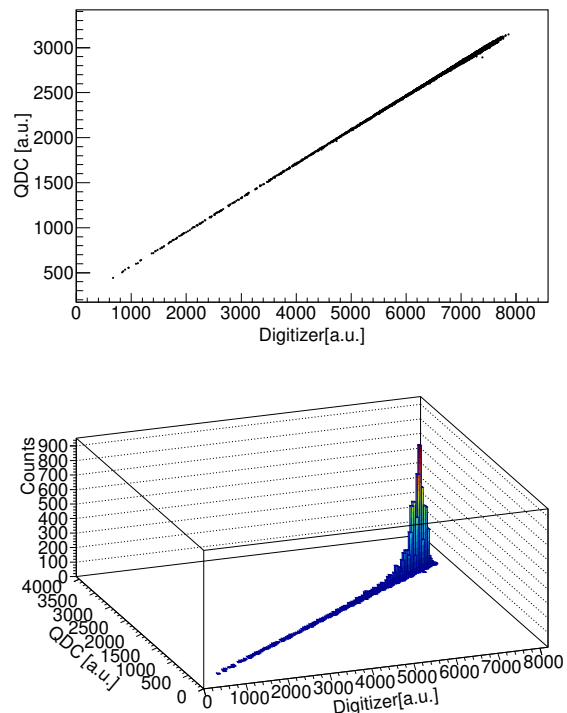


Figure 10. The upper panel shows the energy deposited in the digitizer versus QDC for events identified to belong to the same signal recorded by the QDC and the digitizer for a single crystal. The bottom panel is the 3D histogram plot of the same data.

The other verification for the selected events and to provide a cross-check of the readout schemes is to plot the energy recorded by the digitizer versus the energy recorded by the QDC. As can be seen in Fig. 10 the energies recorded in two different readout schemes are correlated, meaning that we identified digitizer events which correspond to events recorded by the QDC on an event-by-event basis.

In order to further study the detector response two sets of data with four beam energies have been taken with a lead absorber being placed in front of the calorimeter. The lead could be used as a preshower material, and also as a way to reduce the background induced by Møller and Bhabha scattering in the final experiment. One data set was taken with a lead absorber having thickness of 10 mm and the other data set with 20 mm. In both cases the electron beam was centered at central crystal. Figure 11 shows energy deposited in the central crystal for these two data sets compared with the measurement without the lead absorber.

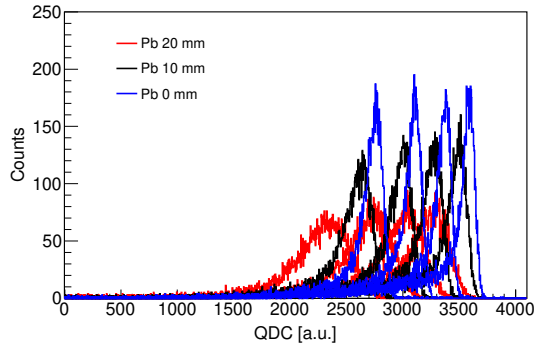


Figure 11. Distribution of energy deposited in the central crystal for the case without a lead absorber and for measurements with lead absorber in front of the calorimeter having thickness of 10 mm and 20 mm.

V. SIMULATION OF TEST BEAM

The simulation for the analysis of the test beam data was developed in Geant4 [6, 7]. We use the FTFP_BERT physics list provided by Geant to simulate the showers and energy loss processes in the crystals. We reproduced the TB24/1 area from the available drawings and technical details provided by DESY. The shielding blocks upstream of the test beam area are 1 m thick, high density concrete. There is a collimator in the wall before area T24 and then there is another collimator in the wall before area TB24/1.

The collimator before TB24/1 is a lead cylinder about 30 cm long and 4 — 6 cm in diameter. The upstream half is 4 cm, and then steps to 6 cm so there is no gap around the edges. Initial runs had a $2\text{ mm} \times 2\text{ mm}$ square collimator hole. For the data presented here we exchanged the collimator with a $8\text{ mm} \times 8\text{ mm}$ square collimator.

About 10 cm from the exit of the collimator is the first pair of trigger detectors. These were adjusted to overlap maximally and are represented as plastic in the simulation. One meter downstream is a second pair of plastic trigger scintillators. Here we overlapped them just by their corners to form a $5\text{ mm} \times 5\text{ mm}$ shape, smaller than the size of a single calorimeter crystal. The trigger scintillators are attached to a movable arm assembly so we can select beam particles that point toward a single crystal. In the simulation we approximate the 4 scintillator trigger assembly as a single plastic scintillator.

The calorimeter is then 10 cm after the second pair of scintillators and has 1 cm of aluminum shielding upstream of the crystals. In the proposed experiment, we will either use lead or aluminum shielding to reduce signals from low energy π 's and e 's. For simplicity we do not include the cooling system in the simulation. The Geant4 visualization of the calorimeter setup is shown in Fig. 12. We do not show the collimator in this figure due to the large distances involved in the simulation.

We show in Fig. 13 a comparison between our QDC

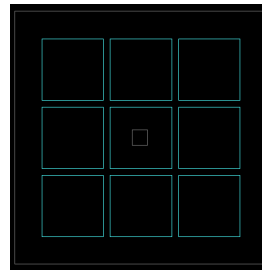


Figure 12. The Geant4 simulation view of the test beam analysis. The perspective is looking downstream toward the front face of the calorimeter. The blue squares are the individual calorimeter crystals which are numbered from 0–8 starting from the top left. The small gray square in the center of the middle crystal is the trigger scintillator, which is upstream of the calorimeter from this perspective. The larger gray square is the aluminum shielding in front of the crystals.

data and the simulation for crystal 4, the central crystal. We require that the incoming particle does not hit the collimator but does strike the trigger scintillator. The data we compare to is pedestal subtracted but has not been energy calibrated. We have rescaled the horizontal axis for ease of viewing. The beam momentum is set to $2\text{ GeV}/c$.

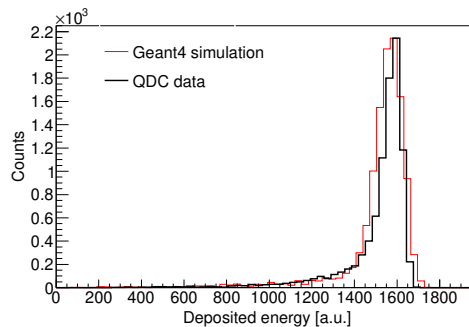


Figure 13. Comparison between Geant4 simulation and data from the QDCs. The simulation is scaled to the height of the data. The data is pedestal subtracted and rescaled horizontally to fit the range of the simulation. The simulation requires the particle does not hit the collimator but does strike the trigger scintillator.

Figure 14 shows a comparison between simulation and our digitizer data. The simulation conditions and that of the data are the same as described in Fig. 13. The events in the digitizer and the QDC were aligned using the timing analysis described above. The discrepancies between simulation and data can be ascribed to an incomplete model of the experimental hall, specifically any material causing energy loss upstream of the hall. We believe with further modeling and technical drawings of the beamline, we would be able to improve agreement between our simulations and data.

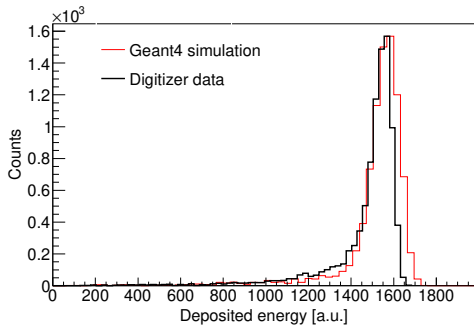


Figure 14. Comparison between Geant4 simulation and data from the digitizers. The simulation is scaled to the height of the data. The data is pedestal subtracted and rescaled horizontally to fit the range of the simulation. The simulation requires the particle does not hit the collimator but does strike the trigger scintillator.

VI. CONCLUSIONS

A prototype, 3×3 , lead tungstate calorimeter was tested at DESY II Test Beam Facility with electron beam having energy 2, 3, 4 and 5 GeV. The signals from PMTs were split in two. One signal was read out using the data acquisition system based on QDC and a signal provided by trigger scintillators and the other signal was read out by signal shape digitizers (streaming readout). Both readout schemes consistently showed slight non-linearity when comparing the beam energy dependence and the position of the total deposited energy peak in calorimeter. This indicates that part of the energy from the primary electron beam is being lost between the individual crystals when it is being converted into the shower of secondary particles. The amount of energy loss tends to be larger for the larger beam energy.

We demonstrated that in the same time digitizer collects more data compared to readout based on QDC. This was also expected, since the QDC requires the trigger signal and also has a dead time and the readout based on digitizer does not have such limitations. Furthermore, by using the time difference between subsequent events, we managed to identify events in a large sample collected by the digitizer which are the same time the events collected by the triggered QDC.

For all four beam energies, data was also taken with a lead absorber being placed in front of the calorimeter. One absorber had thickness of 10 mm and the other of 20 mm. When overlaying the data for all beam energies and absorber thicknesses one can clearly observe a broadening and a movement of the recorded peak towards lower QDC channels if one increases the absorber thickness.

The collected data was also compared with the Geant4 simulation. Due to limited information on the beam path between the storage ring and the calorimeter we were not able to include all the details in the simulation which resulted in some discrepancies between the simulation and the recorded data.

For the future, we plan to perform a new test at the DESY II Test Beam Facility with an improved version of the lead tungstate calorimeter. First, we will increase the number of crystals and build 5×5 , lead tungstate calorimeter. Second, by using a thinner wrapping material the gap between individual crystals will be smaller, hence, undetected energy from the particle shower will be further reduced. The new test measurement will be performed in T24 area, where we will have a detailed knowledge of the beam path from the beam extraction point to the calorimeter and will help us to further improve the Geant4 simulation.

VII. ACKNOWLEDGEMENTS

The measurements leading to these results have been performed at the Test Beam Facility at DESY Hamburg (Germany), a member of the Helmholtz Association (HGF). The setup and operation of these tests were extremely easy and enabled us to achieve everything we needed in a relatively short time thanks to the help of the test beam coordinators: Ralf Diener, Norbert Meyners, and Marcel Stanitzki.

We are very grateful to Tanja Horn of Catholic University of America for loaning us the lead tungstate crystals used in this test. Obviously the tests would not have been possible without her assistance.

We also acknowledge the generous support from several funding agencies without which none of this would be possible. These include: DOE Office of Science grant DE-FG02-94ER4081, PIER Hamburg-MIT/BOS Seed Project PHM-2019-04, and National Science Foundation grant 2012114.

-
- [1] R. Diener *et al.*, *Nucl. Instrum. Meth. A* **922**, 265 (2019), [arXiv:1807.09328 \[physics.ins-det\]](#).
 - [2] R. Abdul Khalek *et al.*, “Science Requirements and Detector Concepts for the Electron-Ion Collider: EIC Yellow Report,” (2021), [arXiv:2103.05419 \[physics.ins-det\]](#).
 - [3] A. Afanasev, P. Blunden, D. Hasell, and B. Raue, *Progress in Particle and Nuclear Physics* **95**, 245 (2017).
 - [4] J. C. Bernauer, *Few Body Syst.* **59**, 116 (2018), [arXiv:1804.06665 \[nucl-ex\]](#).
 - [5] J. C. Bernauer *et al.* (OLYMPUS), *Phys. Rev. Lett.* **126**, 162501 (2021), [arXiv:2008.05349 \[nucl-ex\]](#).
 - [6] S. Agostinelli *et al.* (GEANT4), *Nucl. Instrum. Meth. A* **506**, 250 (2003).
 - [7] J. Allison *et al.*, *Nucl. Instrum. Meth. A* **835**, 186 (2016).
 - [8] T. Horn *et al.*, *Nucl. Instrum. Meth. A* **956**, 163375 (2020), [arXiv:1911.11577 \[physics.ins-det\]](#).
 - [9] A. Asaturyan *et al.*, *Nucl. Instrum. Meth. A* **1013**, 165683 (2021).